

First-order superfluid to Mott-insulator phase transitions in spinor condensates

J. Jiang,^{1,*} L. Zhao,^{1,*} S.-T. Wang,² Z. Chen,¹ T. Tang,¹ L.-M. Duan,² and Y. Liu^{1,†}

¹*Department of Physics, Oklahoma State University, Stillwater, Oklahoma 74078, USA*

²*Department of Physics, University of Michigan, Ann Arbor, Michigan 48109, USA*

(Dated: December 16, 2015)

We observe evidence of first-order superfluid to Mott-insulator quantum phase transitions in a lattice-confined antiferromagnetic spinor Bose-Einstein condensate. The observed signatures include hysteresis effect and significant heatings across the phase transitions. The nature of the phase transitions is found to strongly depend on the ratio of the quadratic Zeeman energy to the spin-dependent interaction. Our observations are qualitatively understood by the mean field theory, and in addition suggest tuning the quadratic Zeeman energy is a new approach to realize superfluid to Mott-insulator phase transitions.

PACS numbers: 67.85.Fg, 03.75.Kk, 03.75.Mn, 05.30.Rt

A quantum phase transition from a superfluid (SF) to a Mott-insulator (MI) was realized in a scalar Bose-Einstein condensate (BEC) trapped by three-dimensional (3D) optical lattices around a decade ago [1]. Marking an important milestone, this achievement has stimulated tremendous efforts to apply highly controllable ultracold bosonic and fermionic systems in studying condensed matter models [2–6]. The SF-MI transitions have been confirmed in various scalar BEC systems via different techniques that can efficiently control the ratio of interatomic interactions to the mobility of atoms [1, 5–7]. One well-known approach to simultaneously enhance interatomic interactions and suppress atomic motion is by raising the depth of an optical lattice [1]. Another convenient method is to manipulate interactions with a magnetically tuned Feshbach resonance [7]. A third technique is to control the hopping energy of bosonic atoms by periodically shaking the lattice [6]. Spinor BECs, on the other hand, possess an additional spin degree of freedom, leading to a range of phenomena absent in scalar BECs [8–13]. One important prediction is the existence of the first-order SF-MI phase transitions in lattice-trapped antiferromagnetic spinor BECs [2, 11, 13–17]. In contrast, the phase transitions can only be second order in scalar BECs and ferromagnetic spinor BECs [2, 5, 17].

In this paper, SF-MI phase transitions are studied in sodium antiferromagnetic spinor BECs confined by cubic optical lattices. We observe hysteresis effect and substantial heating across the phase transitions, which indicate the existence of meta-stable states and associated first-order transitions. In the ground state of the spinor BECs, the nature of the SF-MI transitions is found to be determined by the competition between the quadratic Zeeman energy q_B and the spin-dependent interaction U_2 . At low magnetic fields where U_2 dominates, signatures of first-order transitions are observed. In the opposite limit, the transitions appear to be second order and resemble those occurring in scalar BECs. These qualitative features are explained by our mean-field (MF) calculations. We also study the phase transitions with an initial meta-stable

state and observe stronger heatings across all magnetic fields. Furthermore, our data indicate that a new technique to realize SF-MI transitions is by varying q_B .

Similar to Refs [12, 18], we describe a lattice-trapped $F = 1$ spinor BEC with the Bose-Hubbard model in the lowest band as follows,

$$H = \frac{U_0}{2} \sum_i n_i(n_i - 1) - J \sum_{\langle i,j \rangle, m_F} b_{i,m_F}^\dagger b_{j,m_F} - \mu \sum_i n_i + \frac{U_2}{2} \sum_i (\vec{S}_i^2 - 2n_i) + q_B \sum_{i,m_F} m_F^2 n_{i,m_F}. \quad (1)$$

Here J is the nearest-neighbor hopping energy, $n_i = \sum_{m_F} n_{i,m_F}$, and $n_{i,m_F} = b_{i,m_F}^\dagger b_{i,m_F}$ is the atom number of the m_F hyperfine state at site i . U_0 characterizes the spin-independent interaction, μ is the chemical potential, and \vec{S}_i is the spin operator at site i [19]. U_2 is positive (negative) in $F = 1$ antiferromagnetic (ferromagnetic) spinor BECs, e.g., $U_2 \simeq 0.04U_0$ in our ^{23}Na system [20]. By neglecting the second order term $(b_{i,m_F}^\dagger - \langle b_{i,m_F}^\dagger \rangle)(b_{j,m_F} - \langle b_{j,m_F} \rangle)$ in the hoppings and applying the decoupling MF theory, Eq. (1) can be reduced to a site-independent form [12, 21, 22],

$$H_{\text{MF}} = \frac{U_0}{2} n(n - 1) + \frac{U_2}{2} (\vec{S}^2 - 2n) + q_B \sum_{m_F} m_F^2 n_{m_F} - zJ \sum_{m_F} (\phi_{m_F}^* b_{m_F} + \phi_{m_F} b_{m_F}^\dagger) + zJ |\vec{\phi}|^2 - \mu n \quad (2)$$

with the vector order parameter being $\phi_{m_F} \equiv \langle b_{m_F} \rangle$ and z being the number of nearest neighbors. With spatially uniform superfluids in equilibrium, one can assume ϕ_{m_F} to be real. $\phi_{m_F} = 0$ ($\neq 0$) in the MI (SF) phase.

An antiferromagnetic $F = 1$ spinor BEC of zero magnetization forms a polar superfluid in equilibrium with $\langle \vec{S} \rangle = 0$ [2, 23, 24]. There are two types of polar superfluids: the longitudinal polar (LP) state with $(\phi_1, \phi_0, \phi_{-1}) = \sqrt{\rho_s}(0, 1, 0)$ and the transverse polar

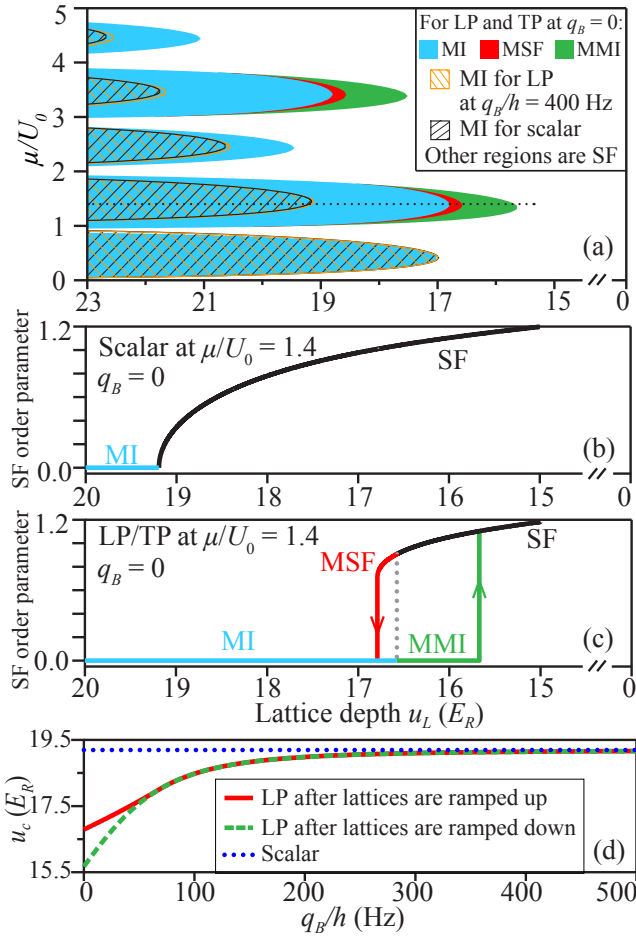


FIG. 1. (Color online) (a) MF phase diagrams derived from the Bose-Hubbard model for scalar BECs [18], and the LP and TP sodium spinor BECs in cubic lattices (see Eq. (2)). The SF order parameter versus u_L in (b) scalar and (c) LP/TP spinor BECs at $\mu/U_0 = 1.4$, i.e., along the dotted line in Panel(a). Note that SF-MI transitions are second order in a scalar BEC, and they are first order showing hysteresis effect in LP and TP spinor BECs at $\mu/U_0 = 1.4$ and $q_B = 0$. (d) Predicted SF-MI transition point u_c versus q_B after cubic lattices are ramped up and down at $\mu/U_0 = 1.4$ (see Eq. (2)).

(TP) state with $(\phi_1, \phi_0, \phi_{-1}) = \sqrt{\rho_s/2}(1, 0, 1)$, where ρ_s is the number of condensed atoms per site. At $q_B = 0$, TP and LP states are degenerate in energy when they have the same ρ_s . At $q_B > 0$, the MF ground state is always the LP state, although a meta-stable TP phase may also exist [2, 24]. We solve Eq. (2) self-consistently by requiring $\phi_{m_F} = \langle b_{m_F} \rangle$ in the occupancy number basis with a maximum of 15 atoms per site. Since the observed peak occupancy number is around six, the truncation errors are negligible.

Our MF calculations show that q_B/U_2 is a key factor to understand the nature of SF-MI transitions in antiferromagnetic spinor BECs. At low magnetic fields (where $0 \leq q_B \lesssim U_2$), U_2 penalizes high-spin configurations and

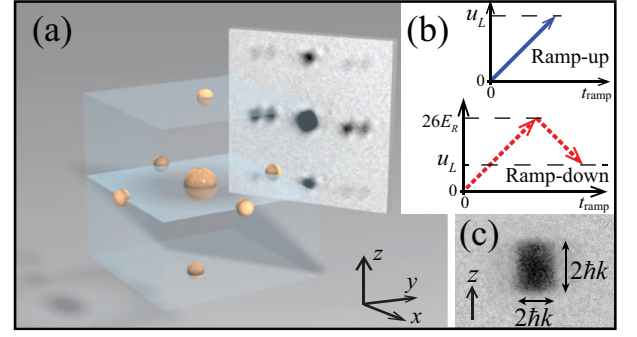


FIG. 2. (Color online) (a) Schematic of the reciprocal lattice and a TOF image taken after lattices are abruptly released. This TOF image is oriented such that its plane is orthogonal to the imaging light. (b) Two lattice ramp sequences used in this paper [25]. (c) A TOF image showing the first Brillouin zone.

enlarges the Mott lobes for even number fillings as atoms can form spin singlets to minimize the energy. Meta-stable Mott-insulator (MMI) and meta-stable superfluid (MSF) phases emerge due to the spin barrier, and lead to first-order SF-MI phase transitions (see Figs. 1(a) and 1(c)) [14, 16, 17]. When 3D lattices are ramped up and down, hysteresis is expected across the phase transitions (i.e., different transition lattice depth u_c). In addition, when the system changes from a meta-stable phase to a stable phase (e.g., from a MSF phase to a MI phase), there will be a jump in the order parameter and the system energy, leading to unavoidable heating to the atoms. Hence, hysteresis and substantial heating may be interpreted as signatures of first-order transitions. As q_B increases, the $m_F = 0$ state has lower energy than other m_F levels and U_2 becomes less relevant. When q_B becomes sufficiently larger than U_2 ($U_2/h \lesssim 80$ Hz in this work), the ground state phase diagram of antiferromagnetic spinor BECs reverts back to one that is similar to the scalar Bose-Hubbard model with only second-order SF-MI transitions (see Figs. 1(a), 1(b) and 1(d)).

Three different types of BECs (i.e., scalar BECs, LP and TP spinor BECs) are studied in this work. A scalar BEC containing up to 1.2×10^5 sodium atoms in the $|F = 1, m_F = -1\rangle$ state is created with an all-optical approach (see Ref. [26]). A $F = 1$ spinor BEC of zero magnetization is then produced by imposing a resonant rf-pulse to the scalar BEC at a fixed q_B . Since the LP state is the MF ground state, it can be prepared by simply holding the spinor BEC for a sufficiently long time at high magnetic fields [24]. A different approach is required to generate the TP state: we apply a resonant microwave pulse to transfer all $m_F = 0$ atoms in the $F = 1$ spinor BEC to the $F = 2$ state, and then blast away these $F = 2$ atoms with a resonant laser pulse. After quenching q_B to a desired value, we adiabatically load the BEC into a cubic lattice by linearly raising the lattice depth u_L

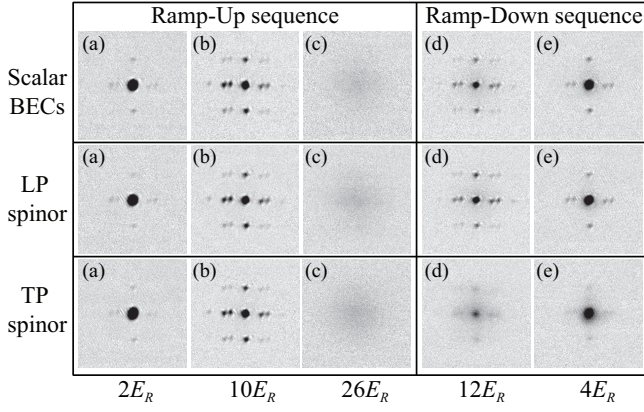


FIG. 3. Interference patterns observed after we abruptly release scalar (top), LP spinor (middle), and TP spinor BECs (bottom) at various u_L and a 5.5-ms TOF at $q_B/h = 360$ Hz. Panels (a)-(c) are taken after ramp-up sequences to a final $u_L = 2, 10$, and $26E_R$, respectively. Panels (d)-(e) are taken after ramp-down sequences to a final u_L of $12E_R$ and $4E_R$. The field of view is $400 \mu\text{m} \times 400 \mu\text{m}$.

within time t_{ramp} [25]. Lattice ramp-up and ramp-down sequences are shown in Fig. 2.

Distinct interference peaks can always be observed during ballistic expansion, after each of the three types of BECs is abruptly released from a shallow lattice of $u_L \leq 10E_R$. Here $E_R = \hbar^2 k_L^2 / (8\pi^2 M)$ is the recoil energy, M and \hbar are respectively the atomic mass and the Planck constant, and k_L is the lattice wave-vector (see Ref. [27]). As shown in the time of flight (TOF) images in Fig. 2(a) and Fig. 3, the six first-order diffracted peaks are symmetrically set apart from the central peak by a distance corresponding to a momentum of $2\hbar k_L$ along three orthogonal axes. These interference peaks may be considered as an indicator for coherence associated with the SF phase in the system. In fact, a larger visibility of interference patterns, a narrower width of the central peak, and a higher optical density (OD) of interference peaks have all been used as trustworthy evidence for improved phase coherence in atomic systems [1, 3, 5, 28]. As an example, the LP spinor BECs studied in Fig. 3 demonstrate long-range phase coherence at $u_L = 10E_R$ with a coherence length of around nine lattice sites, which is estimated from the ratio of the central peak width to $4\hbar k_L$ [3, 5].

Figure 3 displays TOF images at five representative u_L , showing the loss and revival of the interference contrast in both scalar and spinor BECs as cubic lattices are ramped up and down. A quantitative analysis of these TOF images is presented in Fig. 4, demonstrating that the interference peaks (i.e., coherence associated with the SF phase) change in a reversible manner with u_L . First, the interference patterns become more visible as the lattice is made deeper, and reach their peak OD around $10E_R$. This may be due to lattice-enhanced den-

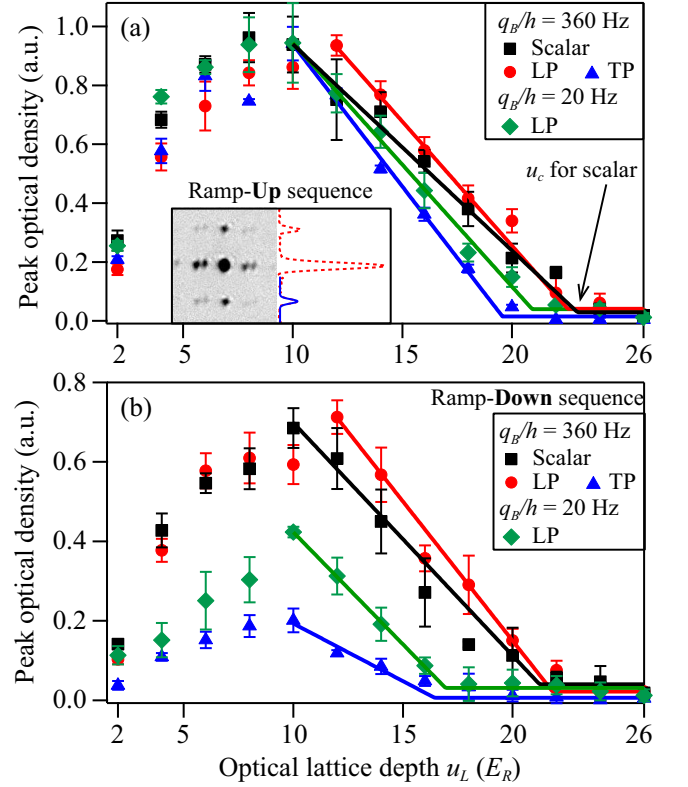


FIG. 4. (Color online) (a) Peak OD of interference peaks as a function of u_L after lattice ramp-up sequences. Markers are experimental data and lines are linear fits. The critical depth u_c is estimated from the intersection of two linear fits to the data. The inset shows how we extract the peak OD from a TOF image (left). The dotted line in the right inset is a density profile of this TOF image through the central and one pair of interference peaks along the vertical direction, while the solid line is a bimodal fit to one side peak. (b) Similar to Panel (a) except that all data are taken after lattice ramp-down sequences.

sity modulation [3, 5, 29]. Second, when u_L is further increased and exceeds a critical value u_c , the interference peaks steadily smear out to a single broad peak indicating atoms completely lose phase coherence. We read off the value of u_c in Fig. 4 from the intersection of two linear fits applied to the data of a given BEC. The loss of coherence can be accounted for by many mechanisms, such as heating, inelastic collisions, or entering into a MI state. To confirm the system has undergone a SF-MI transition, we monitor the lattice ramp-down sequence, because one characteristic of a MI state has proven to be a loss of phase coherence in deep lattices and a subsequent rapid revival of coherence as u_L is reduced [1, 3, 5]. As shown in Fig. 4(b), the interference peaks of both scalar and spinor BECs reversibly revive after the ramp-down sequences, indicating atoms quickly recombine and return to SF states.

Observations in Fig. 4 are qualitatively consistent

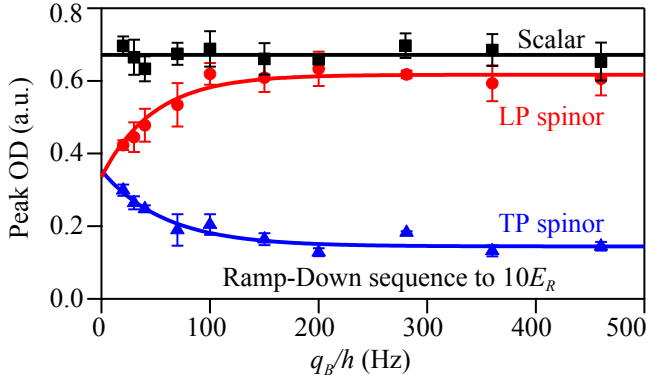


FIG. 5. (Color online) Peak OD of interference peaks as a function of q_B observed after lattice ramp-down sequences to $10E_R$. Markers are experimental data. Red and blue lines are exponential fits. The black line is a linear fit.

with our MF calculations and suggest the existence of first-order SF-MI transitions under some circumstances. First, LP spinor BECs at high magnetic fields possess many properties (e.g., the peak OD) that are similar to those of scalar BECs. Their ramp-up and ramp-down curves are close to each other, while both have roughly symmetric transition points u_c . Similar phenomena were observed in ^{87}Rb and ^6Li systems, and have been considered as signatures of second-order SF-MI transitions [1, 3, 5]. Second, LP states at low magnetic fields and TP states at high fields apparently have smaller u_c for both ramp-up and ramp-down processes compared to scalar BECs, suggesting enlarged Mott lobes. Particularly, the ramp-down u_c for LP states at low fields is noticeably smaller than their ramp-up u_c , corroborating with the MF picture that hysteresis occurs across the first-order phase transitions. Third, the recovered interference contrast is visibly different for various BECs after the ramp-down process (after SF-MI phase transitions). For scalar and high-field LP spinor BECs, nearly 75% of peak OD can be recovered in the interference peaks after the ramp-down sequence. The slightly reduced interference contrast may be due to unaccounted heatings, which leads a small portion of atoms ($< 20\%$) to populate the Brillouin zone. In contrast, after we utilized quite a few techniques and optimized many parameters, the maximal recovered interference contrast of low-field LP states is only $\sim 40\%$ ($\sim 20\%$ for high-field TP states). We attribute this to unavoidable heatings across the first-order transitions as there is a jump in system energy between meta-stable states and stable states. Both hysteresis effect and significant heatings strongly suggest that first-order SF-MI transitions are realized in our experiment. Note, however, we do not see noticeable jumps in the observables as is typically associated with first-order transitions. This is likely due to the presence of even and odd atom fillings in inhomogeneous systems such as trapped

BECs, although the predicted first-order SF-MI transitions only exist for even occupancy number. Limited experimental resolutions may be another reason.

In addition, our data of the LP state in Fig. 4(b) demonstrate the feasibility of realizing SF-MI transitions via a new approach, i.e., by ramping q_B at a fixed lattice depth. For example, when the final u_L in the ramp-down sequence is set at a value between $17E_R$ and $21E_R$, atoms in the LP spinor BECs can cross the SF-MI transitions if q_B is sufficiently reduced (e.g., from $h \times 360$ Hz to $h \times 20$ Hz). This agrees with the MF prediction in Fig. 1(d): u_c depends on q_B in antiferromagnetic spinor BECs.

We then compare scalar and spinor BECs within a wide range of magnetic fields, $20 \text{ Hz} \leq q_B/h \leq 500 \text{ Hz}$, after identical lattice ramp sequences to $u_L = 10E_R$. We choose $10E_R$ because it is apparently the lattice depth around which we observe the maximum interference contrast, with negligible difference in scalar and spinor BECs after the ramp-up sequence at all q_B . This is consistent with Fig. 1, which predicts all BECs studied in this work should be well in the SF phase at $10E_R$. However, the interference peak ODs show intriguing differences after the ramp-down sequence to $10E_R$ (see Fig. 5): deviations from the maximal value appear for LP spinor BECs at low magnetic fields and the TP state at all positive q_B . We again attribute this to different amount of heatings across the SF-MI transitions. Different extent of heatings may be produced due to different spin barriers as well as the amount of energy jump across the transitions. Hence, the maximum recovered OD is a good indicator for the appearance/disappearance of first-order phase transitions. Notably, LP spinor BECs are found to behave very similarly to scalar BECs as long as q_B is large enough, i.e., $q_B \geq h \times 100 \text{ Hz} > U_2$ as shown in Fig. 5. This observation is again consistent with Fig. 1(d), in which the two MF curves for the LP state merge indicating that meta-stable states disappear and SF-MI transitions become second order when $q_B/h > 70$ Hz. Furthermore, the difference between LP and TP spinor BECs appears to exponentially decrease as q_B approaches zero. Exponential fits to the data verify that the LP and TP spinor BECs should show the same behavior at $q_B = 0$.

In conclusion, we have conducted the first experimental study on the SF-MI phase transitions in an antiferromagnetic sodium spinor BEC confined by 3D optical lattices. We have observed the hysteresis effect and significant heatings across the phase transitions, which suggest first-order SF-MI transitions are realized in our experiment. These observations and the dependence of the phase transitions on q_B can be qualitatively understood by MF theory. Further studies are required to confirm more signatures of the first-order transitions, for example by precisely imaging Mott shells [4, 7]. Our data also suggest the feasibility of realizing SF-MI phase transitions via changing the quadratic Zeeman energy.

We thank the ARO and the NSF for financial support. STW and LMD are supported by the IARPA, the ARL, and the AFOSR MURI program. STW thanks Xiaopeng Li for helpful discussions.

* These authors contributed equally to this work.

† yingmei.liu@okstate.edu

- [1] M. Greiner, O. Mandel, T. Esslinger, T. W. Hänsch, and I. Bloch, *Nature* **415**, 39 (2002).
- [2] D. M. Stamper-Kurn and M. Ueda, *Rev. Mod. Phys.* **85**, 1191 (2013).
- [3] J. K. Chin, D. E. Miller, Y. Liu, C. Stan, W. Setiawan, C. Sanner, K. Xu, and W. Ketterle, *Nature* **443**, 961 (2006).
- [4] G. K. Campbell, J. Mun, M. Boyd, P. Medley, A. E. Leanhardt, L. G. Marcassa, D. E. Pritchard, and W. Ketterle, *Science* **313**, 649 (2006).
- [5] I. Bloch, J. Dalibard, and W. Zwerger, *Rev. Mod. Phys.* **80**, 885 (2008).
- [6] H. Lignier, C. Sias, D. Ciampini, Y. Singh, A. Zenesini, O. Morsch, and E. Arimondo, *Phys. Rev. Lett.* **99**, 220403 (2007).
- [7] C. Chin, R. Grimm, P. Julienne, and E. Tiesinga, *Rev. Mod. Phys.* **82**, 1225 (2010).
- [8] P. Windpassinger, and K. Sengstock, *Rep. Prog. Phys.* **76**, 086401 (2013).
- [9] J. Heinze, S. Götze, J. S. Krauser, B. Hundt, N. Fläschner, D.-S. Lühmann, C. Becker, and K. Sengstock, *Phys. Rev. Lett.* **107**, 135303 (2011).
- [10] P. Soltan-Panahi, J. Struck, P. Hauke, A. Bick, W. Plenkers, G. Meineke, C. Becker, P. Windpassinger, M. Lewenstein, and K. Sengstock, *Nat. Phys.* **7**, 434 (2011).
- [11] G. G. Batrouni, V. G. Rousseau, and R. T. Scalettar, *Phys. Rev. Lett.* **102**, 140402 (2009).
- [12] K. W. Mahmud and E. Tiesinga, *Phys. Rev. A* **88**, 023602 (2013).
- [13] S. S. Natu, J. H. Pixley, and S. Das Sarma, *Phys. Rev. A* **91**, 043620 (2015).
- [14] E. Demler and F. Zhou, *Phys. Rev. Lett.* **88**, 163001 (2002).
- [15] A. Imambekov, M. Lukin, and E. Demler, *Phys. Rev. A* **68**, 063602 (2003).
- [16] K. V. Krutitsky, M. Timmer, and R. Graham, *Phys. Rev. A* **71**, 033623 (2005).
- [17] T. Kimura, S. Tsuchiya, and S. Kurihara, *Phys. Rev. Lett.* **94**, 110403 (2005).
- [18] M. P. A. Fisher, P. B. Weichman, G. Grinstein, and D. S. Fisher, *Phys. Rev. B* **40**, 546 (1989).
- [19] The linear Zeeman energy is ignored in Eq. (1), since it remains the same during collisional spin interconversions in $F = 1$ spinor BECs. The spin operators at site i are given by

$$S_{ix} = \frac{1}{\sqrt{2}} \left(b_{i,0}^\dagger b_{i,1} + b_{i,1}^\dagger b_{i,0} + b_{i,-1}^\dagger b_{i,0} + b_{i,0}^\dagger b_{i,-1} \right),$$

$$S_{iy} = \frac{i}{\sqrt{2}} \left(b_{i,0}^\dagger b_{i,1} - b_{i,1}^\dagger b_{i,0} + b_{i,-1}^\dagger b_{i,0} - b_{i,0}^\dagger b_{i,-1} \right),$$

$$S_{iz} = b_{i,1}^\dagger b_{i,1} - b_{i,-1}^\dagger b_{i,-1}.$$
- [20] L. Zhao, J. Jiang, T. Tang, M. Webb, and Y. Liu, *Phys. Rev. Lett.* **114**, 225302 (2015).
- [21] R. V. Pai, K. Sheshadri, and R. Pandit, *Phys. Rev. B* **77**, 014503 (2008).
- [22] A. Wagner, *Spinor condensates in optical superlattices*, Ph.D. thesis, University of Basel (2012).
- [23] T.-L. Ho, *Phys. Rev. Lett.* **81**, 742 (1998).
- [24] J. Jiang, L. Zhao, M. Webb, and Y. Liu, *Phys. Rev. A* **90**, 023610 (2014).
- [25] Lattices are linearly ramped up to a given u_L in a ramp-up sequence, while lattices are first adiabatically ramped up to $26E_R$ and then back down to a variable final u_L in a ramp-down sequence. We find that a ramp speed of $2E_R/\text{ms}$ is sufficient to satisfy the intraband adiabaticity condition and ensure $\geq 80\%$ of atoms remain in a scalar or a high-field LP spinor BEC after a ramp-down sequence to $2E_R$.
- [26] L. Zhao, J. Jiang, T. Tang, M. Webb, and Y. Liu, *Phys. Rev. A* **89**, 023608 (2014).
- [27] The 3D optical lattice is constructed by three optical standing waves from a single-mode laser at 1064 nm, which results in a cubic periodic potential with a lattice spacing of 532 nm. All lattice beams are frequency-shifted by at least 20 MHz with respect to each other for eliminating cross interference among them. The calibration of u_L is conducted via Kapitza-Dirac diffraction patterns and has an uncertainty of $\sim 15\%$.
- [28] R. B. Diener, Q. Zhou, H. Zhai, and T.-L. Ho, *Phys. Rev. Lett.* **98**, 180404 (2007).
- [29] K. Xu, Y. Liu, D. E. Miller, J. K. Chin, W. Setiawan and W. Ketterle, *Phys. Rev. Lett.* **96**, 180405 (2006).